ACS APPLIED MATERIALS & INTERFACES

Research Article

Cite This: ACS Appl. Mater. Interfaces 2018, 10, 2907−2917

www.acsami.org

Environmentally Benign Production of Stretchable and Robust Superhydrophobic Silicone Monoliths

Alexander Davis,*[,†] Salvatore Surdo,[‡] Gianvito Caputo,[†] Ilker S. Bayer,*[,†] and Athanassia Athanassiou*[,†]

[†]Smart Materials, Istituto Italiano di Tecnologia, Genoa 16163, Italy

[‡]Nanophysics Department, Istituto Italiano di Tecnologia, Genoa 16163, Italy

Supporting Information

ABSTRACT: Superhydrophobic materials hold an enormous potential in sectors as important as aerospace, food industries, or biomedicine. Despite this great promise, the lack of environmentally friendly production methods and limited robustness remain the two most pertinent barriers to the scalability, large-area production, and widespread use of superhydrophobic materials. In this work, highly robust superhydrophobic silicone monoliths are produced through a scalable and environmentally friendly emulsion technique. It is first found that stable and surfactantless water-in-polydimethylsiloxane (PDMS) emulsions can be formed through mechanical mixing. Increasing the internal phase fraction of the precursor emulsion is found to increase porosity and microtexture of the final monoliths, rendering them superhydrophobic. Silica nanoparticles can also be dispersed in the aqueous internal phase to create micro/nanotextured monoliths, giving further improvements in superhydrophobicity. Due to the elastomeric nature of PDMS, superhydrophobicity can be maintained even while the material is mechanically strained or compressed. In addition, because of their self-similarity, the monoliths show outstanding robustness to knife-scratch, tape-peel, and finger-wipe tests, as well as rigorous sandpaper abrasion. Superhydrophobicity was also unchanged when exposed to adverse environmental conditions including corrosive solutions, UV light, extreme temperatures, and high-energy droplet impact. Finally, important properties for eventual adoption in real-world applications including self-cleaning, stain-repellence, and blood-repellence are demonstrated.

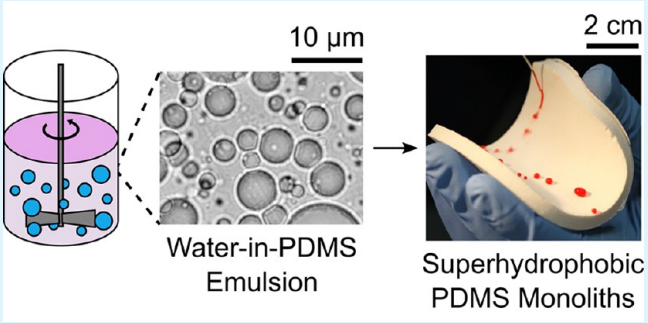

KEYWORDS: *superhydrophobic, porous PDMS, wear-resistance, water-based fabrication*

1. INTRODUCTION

Free-standing superhydrophobic materials have drawn great interest due to their wide range of possible applications including self-cleaning and stain-repellent films,[1] hydraulic[2,3] and biomedical[4,5] tubing with reduced drag, pumpless microfluidic circuits,[6−8] and anti-icing tapes.[9,10] While a diverse array of materials and techniques have been reported that produce the surface roughness and hydrophobic chemical functionality necessary for superhydrophobicity,[11,12] two important challenges have been commonly identified that must be overcome before superhydrophobic materials can be successfully produced and utilized in real-world settings.

First is the need for environmentally friendly ("green") techniques for the mass production of superhydrophobic surfaces. Namely, the use of fluorinated substances and volatile organic compounds (VOCs) must be limited in the production of liquid repellent surfaces. Fluorinated chains confer the lowest surface energy of any type of surface chemical functionality and thus, when applied to the appropriate surface texture, can render a surface superhydrophobic.[13] However, fluorinated compounds have also been identified as a source of toxic pollutants which persist in the environment.[14?] It is therefore desired to design processes for the production of superhydrophobic materials that do not include the use of fluorinated substances. However, VOCs are ubiquitous in the fabrication of superhydrophobic materials because they readily dissolve hydrophobic species, and in the case of polymer based spray coatings, the quick evaporation of VOCs promotes the creation of hierarchical texture. However, they are known toxins and irritants whose large-scale use is restricted by law. While there have been recent reports of processes which utilize nonfluorinated[15−19] or waterborne materials,[20−22] there have been relatively few reports of production techniques in which both are employed. Notable examples include waterborne spray coatings of polyolefin/exfoliated graphite nanoplatelets,[23] polyolefin/TiO_2,[24] and PU/silanized palygorskite nanorods.[25] Besides spray formulations, it has been shown that cured silicone sealants can be embedded with hydrophobic soot

Received: October 5, 2017
Accepted: December 29, 2017
Published: December 29, 2017

DOI: 10.1021/acsami.7b15088
ACS Appl. Mater. Interfaces 2018, 10, 2907−2917

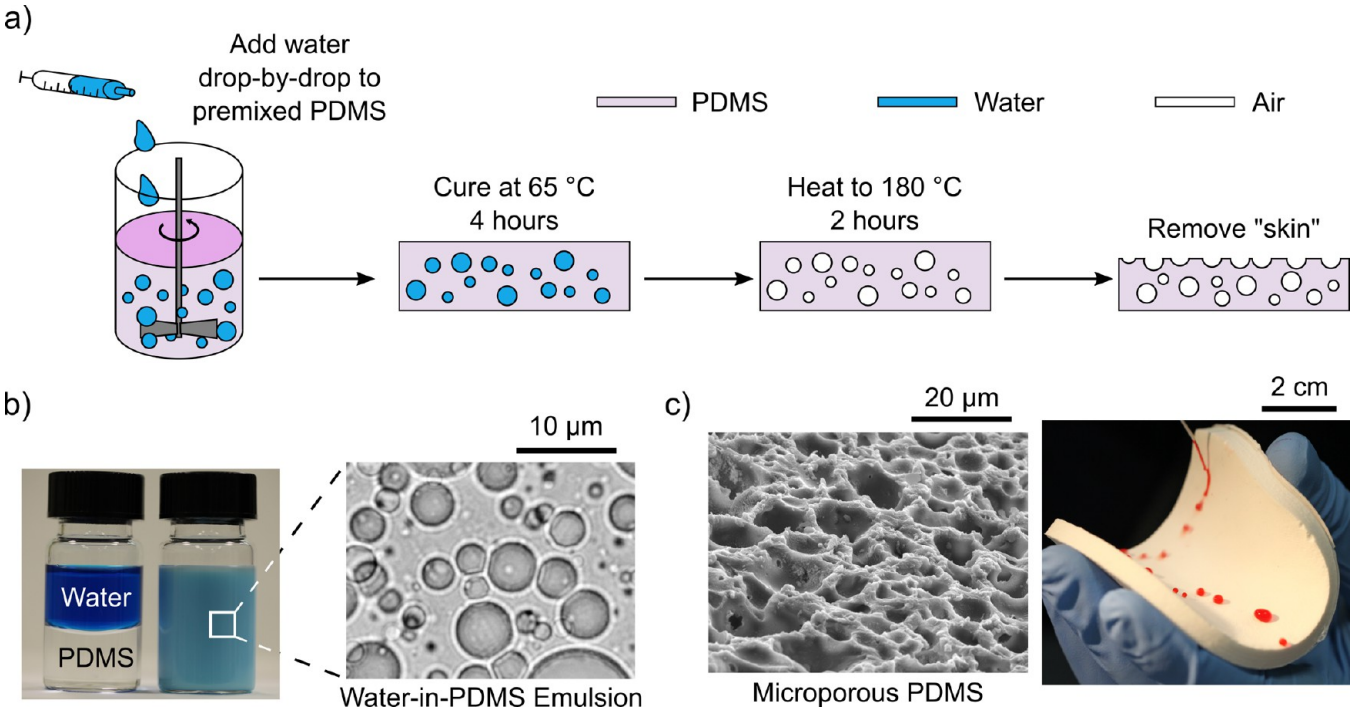

Figure 1. a) Scheme of the emulsion templating process used to produce microtextured PDMS monoliths. Surfactantless water-in-PDMS emulsions are first obtained by mechanical mixing. After heat curing the PDMS external phase, the solid monolith is heated to force trapped water to evaporate. Bulk microtexture is revealed after sanding. b) Photographs of vials containing phase separated water (dyed blue for contrast) and PDMS, and the water-in-PDMS emulsion. An optical micrograph of the emulsion reveals well-dispersed water microdroplets. c) SEM image of a cured monolith shows the microtexture imparted by emulsion templating. Impacting water droplets (dyed red for contrast) showed high mobility on the microtextured surface.

particles when exposed to premixed flames or elevated temperatures.[26,27]

Second, although several low-cost and large-scale methods have been developed to fabricate superhydrophobic materials, maintaining superhydrophobic performance when subjected to harsh mechanical treatment (e.g., stretching, compressing, and surface wear) and environmental conditions (e.g., corrosive liquids, UV exposure, and extreme temperatures) remains one of the most difficult obstacles for their eventual widespread use in industrial settings.[28] In particular, mechanical surface abrasion has been shown to cause droplets to lose their mobility on superhydrophobic surfaces (i.e., Cassie to Wenzel transition).[29] Wear-resistance has most commonly been tested by sandpaper abrasion, although relatively low applied loads (<5 kPa)[30−40] or short abrasion distances (<10 m)[26,41−45] have typically been reported. As the degradation of superhydrophobicity during abrasion can be attributed to a destruction/flattening of surface features, self-similar materials such as foams or layer-by-layer coatings, which exhibit superhydrophobicity not only at the top surface but also at any revealed cross section throughout the bulk of the material, have been identified as the appropriate structure for wear-resistant superhydrophobicity that can be maintained even after mechanical surface abrasion.[46,47]

Polymer emulsion templating is a simple and scalable method for producing porous monoliths.[48−53] In this process, surfactant stabilized emulsions are first formed with water and a water-soluble initiator as the internal phase and a monomer as the external phase. Polymerization is then allowed to proceed and after water, excess surfactant, and unreacted monomer are removed, a microcellular polymer foam is obtained. While emulsion polymerization has been used to produce particles that can form superhydrophobic coatings,[54−56] to the authors' knowledge, polymer emulsion templating has not yet been used to make free-standing superhydrophobic materials with bulk porosity. In this work, we present bulk superhydrophobic silicone elastomers produced through emulsion templating. The effect of the initial emulsion composition on the resulting monolith was investigated, with hydrophobicity increasing with increasing internal phase fraction (responsible for microtexture). Dispersing silica nanoparticles in the internal phase (responsible for nanotexture) brought further improvements to water repellency. The monoliths maintained superhydrophobicity even when subjected to a wide variety of mechanical robustness tests include stretching, compression, abrasion, knife-scratch, tape-peel, and finger-wipe, as well as when exposed to acid/base solutions, UV light, high temperatures, and high-energy droplet impact. Besides exhibiting robust superhydrophobicity, the monoliths were also observed to have excellent self-cleaning, stain-repellence, and blood-repellence properties, making them useful for a wide range of applications.

2. MATERIALS AND METHODS

2.1. Fabrication of Porous Silicone Monoliths. PDMS elastomers have gained widespread use as the starting point for free-standing superhydrophobic materials because, in addition to their exceedingly low surface free energy (γ_{sv} = 20 mJ/m^2), they are cost-effective, readily available, biocompatible, and flexible. However, textured PDMS elastomers generally rely on soft lithography with molds made using time-consuming and complex processes such as photolithography,[57,58] plasma[59,60] or acid etching,[61] or laser ablation,[62] as well as incorporating hydrophobic nanofillers dispersed in organic solvents.[63,64] In addition the texture produced using these techniques only exists at the top surface, not throughout the bulk of the material. Sylgard 182 (Dow Corning) has the same final mechanical and wetting

DOI: 10.1021/acsami.7b15088
ACS Appl. Mater. Interfaces 2018, 10, 2907−2917

properties as the commonly used Sylgard 184. However, while Sylgard 184 can fully cure at room temperature and has a pot-life of 2 h, Sylgard 182 requires heating to fully cross-link and has a longer pot-life at room temperature (8 h). As the emulsification process described here can take longer than the pot life of Sylgard 184 depending on the volume ratios of the water-in-PDMS emulsions, it was chosen to use Sylgard 182 rather than Sylgard 184 to fabricate porous PDMS in order to avoiding PDMS cross-linking during emulsification.

A scheme of the process to fabricate microtextured PDMS is shown in Figure 1a. The base and curing agent of Sylgard 182 were first mixed in a 10:1 ratio (w:w) in a 500 mL polypropylene beaker. Water was then added dropwise using a syringe pump to the uncured PDMS at a rate of 30 mL/h under stirring using an overhead stirrer (RZR 2051, Heidolph) with a stainless steel propeller-type impeller (PR 30) at a speed of 600 rpm. Interestingly, no surfactant or electrolyte needed to be added for emulsification. This drastically reduced the overall complexity of the process, as typically Soxhlet extraction must be done after polymerization in order to remove surfactant. To fabricate microtextured monoliths, emulsions were made with internal phase wt % ranging from 10% to 70% in 10% increments. As water was added to the uncured PDMS, a white, creamy emulsion formed. A photo of a phase-separated water/PDMS mixture and the 50% emulsion (with water colored blue for better clarity) is shown Figure 1b. The viscosity of the final emulsion was observed to increase with increasing internal phase fraction. In particular, the 70% emulsion had a paste-like consistency and was no longer self-leveling. The 60% emulsion was thus chosen as the basis for the micro/nanostructured monoliths because it contained the highest internal phase fraction while still maintaining good flow characteristics. To fabricate micro/nanotextured monoliths, hydrophilic fumed silica (10 nm primary particle size, Aerosil 300, Evonik) was first dispersed in water through probe sonication (VCX-750, Sonics & Materials), and emulsification was carried out as in the case of the microtextured monoliths. Dispersions were made in order to produce final monoliths containing 1%, 5%, and 10% by weight silica on a dry basis. The emulsion was then poured in a polystyrene Petri dish to serve as a mold and degassed in a vacuum desiccator. The time for degassing depended on the internal phase fraction of the emulsion because of the increase in viscosity with increasing water content. Roughly 1 h was needed to degas the 10% emulsion and 5 h to degas the 70% emulsion. After degassing the polystyrene dish was sealed, and the emulsion was placed in an oven at 65 °C for 4 h to allow the PDMS to cure. The polystyrene dish was sealed to prevent water from evaporating while the PDMS cured. The cured elastomer was then released from the polystyrene dish, and the water inside the sample was forced to evaporate by heating in an oven at 180 °C for 2 h. A nontextured "skin" was always observed to remain around the periphery of the material (Figure S1 of the Supporting Information, SI). Therefore, the dried porous elastomer was then sanded with 120 grit sandpaper in order to reveal its bulk texture, as can be seen in Figure 1c.

2.2. Characterization. *2.2.1. Morphological Characterization.* Scanning electron microscope (SEM) images of the produced monoliths were acquired using a JEOL JSM-6490LA microscope working in high-vacuum mode with an accelerating voltage of 10 kV. Samples were sputter coated with a 10 nm thick layer of gold before imaging to reduce charging effects. SEM images of uniaxially stretched monoliths were obtained by stretching samples with a mechanical vise, sputter coating, and inserting the entire assembly into the SEM chamber to image the sample while stretched. The three-dimensional morphology of the monoliths was studied using a confocal laser scanning microscope (Nikon A1R). In particular, volumetric images (voxel size 0.15 μm^3) were acquired by scanning samples with a 488 nm laser, and the reflected light was collected with a microscope objective (Nikon Plan Apo, 20X-0.75NA). Three-dimensional images were then processed with homemade software in order to estimate the roughness, i.e., peak to valley values (R_{PV}), of the monoliths. The procedure was repeated three times for each internal phase wt % to obtain the average and standard deviation of R_{PV}.

2.2.2. Wettability Characterization. In order to measure contact angle (CA), images of sessile droplets were first acquired using a contact angle goniometer (OCA 20, Dataphysics), and then analyzed using the Drop Shape Analysis plugin for ImageJ.[65] Roll-off angle (ROA) was measured using the aforementioned goniometer, with the stage tilting at a rate of 1 deg/s. Three measurements of each type were conducted on each sample using 5 μL droplets, and their average, minimum, and maximum values are reported. Wetting measurements of uniaxially stretched samples were performed using the vise described in Section 2.2.1. In addition, the antiwetting property of a microtextured PDMS sample was examined while being biaxially stretched using a custom-made stretching device (see SI for details).

2.2.3. Chemical Characterization. X-ray photoelectron spectroscopy (XPS) measurements were performed using a SPECS XPS spectrometer equipped with a nonmonochromatic AlKα anode as X-ray source ($h\nu$ = 1486.6 eV) operated at 15 kV and 10 mA. The C 1s spectral components were charge-corrected at 284.4 eV. The spectra were then analyzed using CasaXPS software.

2.2.4. Mechanical Robustness Characterization. Stress−strain curves were obtained using an Instron 3365 uniaxial tension tester operating at a strain rate of 200%/min and equipped with a noncontacting video extensometer. To find Young's modulus and maximum elongation, 10 measurements were recorded for an untreated, microtextured, and micro/nanotextured PDMS sample, with the mean and standard deviation reported. To investigate resistance of the surface structure to compression, a micro/nanotextured sample 1.2 cm in diameter was placed in a hydraulic press (CrushIR, Pike) with 200 kg of force applied (17 MPa pressure). The use of standard and reproducible wear tests is of crucial importance for the accurate characterization of the mechanical wear-resistance of superhydrophobic materials. Here, a test was developed that conforms to the guidelines of best practice described by Tian et al.[66] First, a circular sample 1.6 cm in diameter was cut out of a larger monolithic sample using a hollow puncher. The circular sample was then placed face down on sandpaper attached to a disc polishing machine (Labpol Duo 8, EXTEC), and a 400 g load was placed on top to create a pressure of 20 kPa. The sandpaper disc was then allowed to rotate while the sample was held fixed, creating friction at the interface. The sample was placed at a radius of 5 cm from the center of the sandpaper disc, which rotated at 3.2 rpm, giving a linear interfacial velocity of 1 m/min. The test was carried out on a microtextured (60 wt % water) and micro/nanotextured (60 wt % water, 10 wt % silica) sample using two sandpaper grits: P240 (average particle diameter = 58.5 μm) and P600 (average particle diameter = 25.8 μm). After every 5 m of linear distance traversed the sample was cleared of debris by rinsing with ethanol and blowing with N_2 and wetting measurements were performed. Wear cycles were performed until 50 m of linear distance were traversed. The wear test was performed up to this point because it was observed that, in the case of the test involving P240 sandpaper, the entire thickness of the test sample (~5 mm) was nearly worn through at this point.

2.2.5. Environmental Robustness Characterization. Chemical resistance was investigated by immersing micro/nanotextured samples in 0.1 M HCl (pH = 1) and 1.0 M NaOH (pH = 14) solutions for 1 h and subsequently measuring the wetting properties of water. UV stability was tested by placing a superhydrophobic monolith in a bromograph (MF 1030/C, Nuova Delta Elettronica) and exposing it to UV light (λ = 320−375 nm, 4.15 mW/cm^2). To investigate temperature resistance, superhydrophobic samples were heated inside of a furnace at temperatures from 250 °C to 350 °C in increments of 50 °C. To test for resistance against high-energy droplet impact a ~20 μL water droplet (diameter = 3.5 mm) was dispensed from a height of approximately 15 cm above a micro/nanotextured sampled inclined to 45°. The interaction between the impacting droplet and superhydrophobic surface was recorded using a high-speed camera (NX4-S2, IDT) at 2000 frames per second. On the basis of analysis of the high-speed videos, the droplet impact velocity was experimentally found to be ~2 m/s, corresponding to a Weber number of We = 200.

2.2.6. Self-Cleaning, Stain-Repellence, and Blood-Repellence Tests. The self-cleaning property of the superhydrophobic monoliths was investigated by first spreading a fouling agent (cocoa powder was used to simulate dirt) on an inclined sample, and then ejecting water

DOI: 10.1021/acsami.7b15088
ACS Appl. Mater. Interfaces 2018, 10, 2907−2917

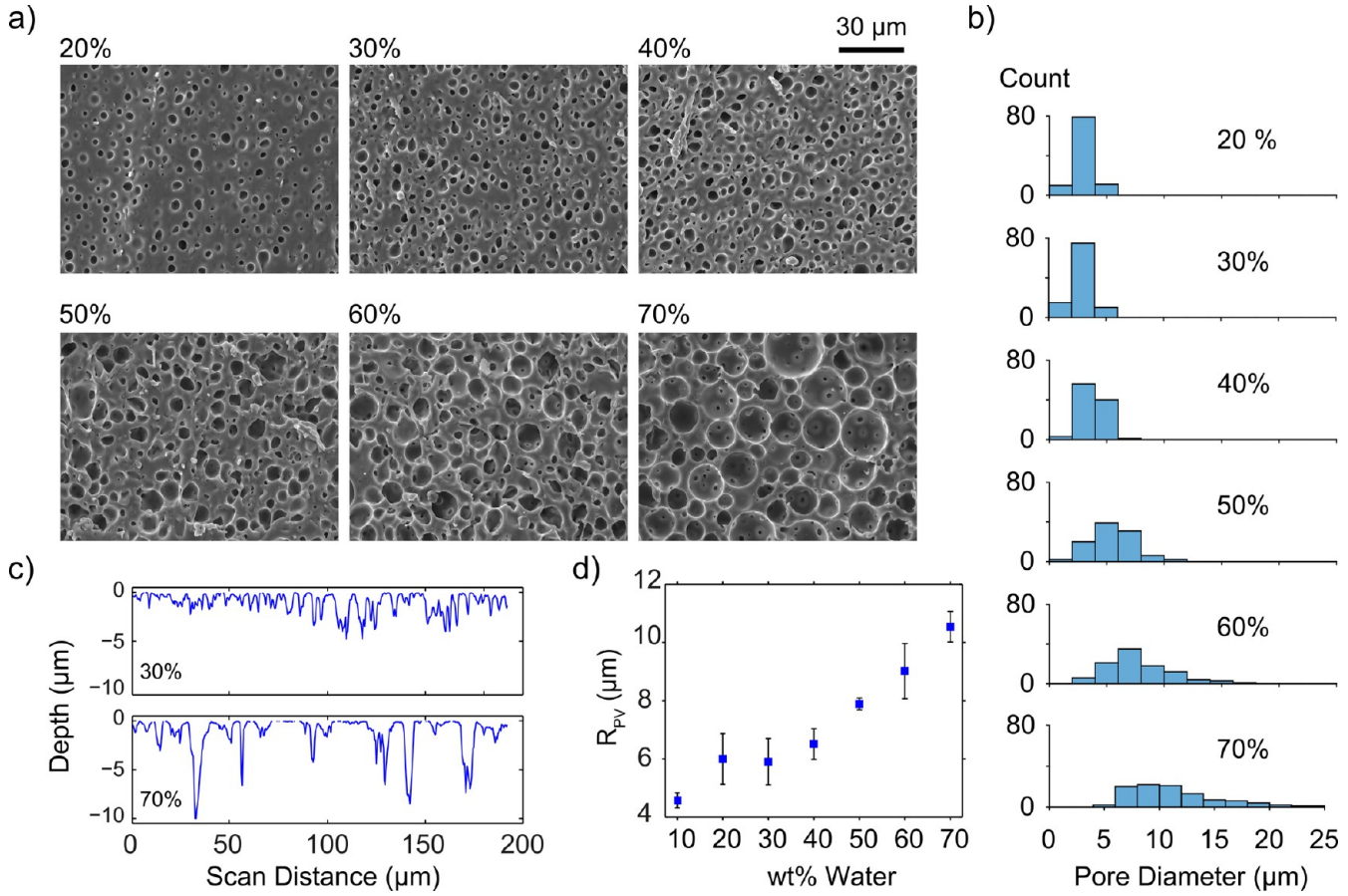

Figure 2. a) SEM images of the microtextured silicones showed increased surface texture with increasing water wt % in the precursor emulsion. b) Histograms of pore diameter showed pore size average and spread increased with increasing water wt %. c) Representative depth profiles of monoliths made from emulsions with 30 and 70 wt % water. d) Peak to valley values increased with water wt % of the precursor emulsion.

droplets onto the fouled area to observe if the powder is taken away with passing droplets. To test for stain-repellence, ~10 μL red wine, coffee, orange juice, and vinegar droplets were dispensed toward a sample surface from a height of 5 cm, with their motion over the surface recorded at 200 frames per second. To investigate blood-repellency, the contact angle of a 7 μL mouse blood droplet was measured on a micro/nanotextured monolith. The dynamic motion of a dispensed blood droplet onto a superhydrophobic surface tilted to 20° was recorded using high-speed videography at 1000 frames per second. Fresh mouse blood was obtained and used in accordance with the guidelines established by the European Communities Council Directive (2010/63/EU) and approved by the National Council on Animal Care of the Italian Ministry of Health. Heparin sodium salt (Sigma-Aldrich) was mixed to the blood (1:10 by volume) and used as anticoagulant to prevent formation of blood clots.

3. RESULTS

Optical microscopy analysis of the developed emulsions revealed that microdroplets of water were observed to be well dispersed throughout the PDMS external phase, with distance between droplets decreasing as water content increased. Optical microscopy images of emulsions with different water wt % are shown in Figure S2. Histograms of the water droplet diameters in each of the emulsions showed that the average value and spread increased as water content increased. At wt % less than 50%, average droplet size was observed to be less than 3 μm. The smallest average diameters observed were in the 30% and 40% emulsions; each of these showed average diameters of 2.4 μm and standard deviation 0.5 μm. When water content was increased to over 50% there was an increase in the average value and spread of diameters, with the 70% emulsion showing the largest average diameter of 5.0 μm and standard deviation 1.3 μm. The stability of a 50% emulsion (made without PDMS cross-linker) was checked 1, 3, and 7 days after initial emulsification. As can be seen in Figure S3, average water droplet size made a substantial increase after 1 day from 2.7 to 8.3 μm. However, after this initial increase droplet size remained fairly constant, and was measured to be 8.1 μm after 7 days. Importantly, no phase separation was observed between the water and PDMS even after 7 days, indicating the stability of the emulsion.

SEM images of the cured microtextured PDMS can be seen in Figure 2a. As expected, as the water content of the starting emulsion increased pores density increased. Starting at 10%, sparse and isolated pores were visible. Increasing the water content, pore density, and interconnectivity increased, with a honeycomb-like structure observed at 70%. This morphology is similar to one achieved in PDMS by molding on top of a rose petal.[67] However, the morphology produced by emulsion templating exists throughout the entire bulk of the material, while molding only affects the top layer. Histograms of pore size in the cured samples are shown in Figure 2b. As was the case when examining the water droplet size in the emulsions, pore size was nearly constant for cured monoliths made from emulsions with water content less than 50%. In this range the 40% PDMS showed the largest average pore size of 3.7 μm. When emulsions with over 50% water content were used, pore

DOI: 10.1021/acsami.7b15088
ACS Appl. Mater. Interfaces 2018, 10, 2907−2917

size increased drastically, with the 70% PDMS showing an average pore size of 11.7 μm. These increased pore sizes with respect to the droplets' diameter in the emulsions were most likely caused by droplet coalescence, when the emulsions were heated to initiate curing. Representative depth profiles obtained using confocal microscopy are shown in Figure 2c. Comparing the scans of the monoliths made from 30% (top) and 70% (bottom) emulsions, it is clear that a higher internal phase fraction produced a rougher surface with a higher variation in surface features. A plot of R_{PV} against water wt % (Figure 2d) showed this as a consistent trend. At water wt % less than 40%, R_{PV} was calculated to be less than 7 μm for all monoliths. Emulsions with higher wt % produced rougher monoliths, with the 70% sample showing R_{PV} greater than 10 μm.

Silica nanoparticles were dispersed in the aqueous internal phase of the 60% emulsions in an effort to impart nanotexture to the pore walls. SEM images of a monolith with 10 wt % silica with respect to PDMS is shown in Figure 3a. In addition to the

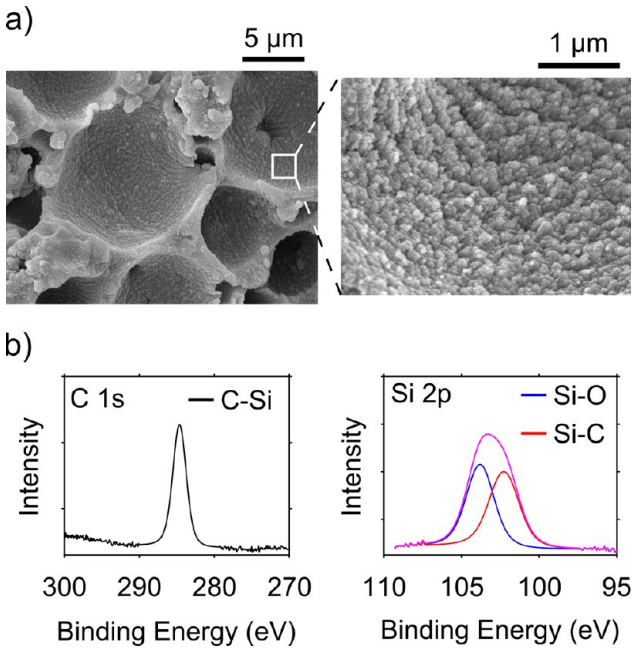

Figure 3. a) SEM images of a micro/nanotextured monolith, with nanotextured pore walls visible at high magnification. b) XPS scans of a micro/nanotextured monolith with prominent C−Si and Si−C peaks, indicating the presence of PDMS at the surface.

microtexture produced by the emulsified water droplets, a clear nanotexture was visible in the PDMS, attributed to silica aggregating at the water/PDMS emulsion interface before and during curing. A similar process carried out using alumina (13 nm primary particle size) and iron(III) oxide (200 nm primary particle size). However, neither was observed to aggregate at the pore walls and produce nanotexture (Figure S4). XPS scans of a micro/nanotextured monolith were performed to check whether the silica nanoparticles were the only component of the surface of the pore walls, or if PDMS was also present. As seen in Figure 3b, both the C−Si peak of the C 1s spectrum and Si−C peak of the Si 2p spectrum were present, indicating that PDMS was still present at the surface of the micro/nanotextured monoliths.

Figure 4 shows the water contact angle and roll-off angle of each of the micro- and micro/nanotextured PDMS samples. To

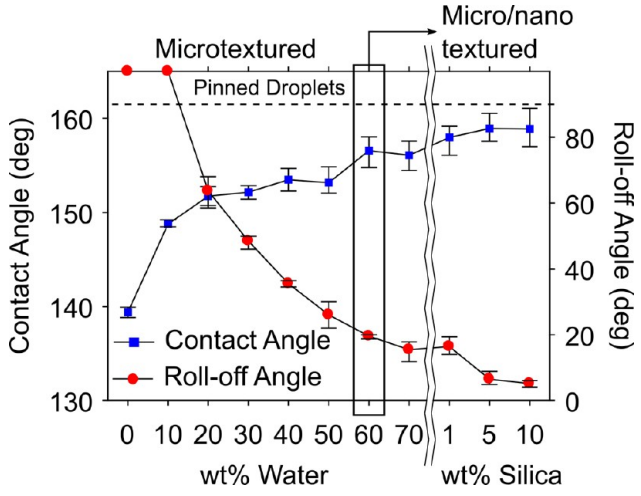

Figure 4. Contact angle and roll-off angle of the silicone monoliths. Wettability was observed to decrease with increasing water wt % in the precursor emulsion due to increased microtexture. Dispersing silica nanoparticles in the water of the precursor produced monoliths with micro/nanotexture and brought about further decreases in wettability.

control for the effect of the sandpaper abrasion needed to reveal the bulk microtexture on the wettability results, a plain PDMS sample was abraded as was done with the porous samples. With this abrasion only, contact angle was observed to be 139°. This was a considerable increase over untreated PDMS, which shows a contact angle of about 105°. For the least porous PDMS (10 wt % internal phase fraction), the contact angle was even higher (148°). However, droplets on each of these surfaces remained pinned when the surface was tilted. Starting at the 20% sample, droplets became mobile on the surface, and contact angle rose to above 150°. The highest contact angle observed among the microtextured PDMS was 156° for the 60% and 70% samples. Roll-off angle was also observed to decrease as porosity increased, reaching a minimum of 15° for the 70% sample. Although droplets were already observed to have high mobility on the microtextured PDMS, the addition of nanotexture to the pore walls brought about even further reduction in liquid−solid adhesion. As can be seen in Figure 4, with increasing amount of silica nanoparticles dispersed in the internal phase of the initial emulsions, an increase in contact angle and decrease in roll-off angle was observed. The monolith with 10 wt % silica with respect to PDMS exhibited the most superhydrophobic behavior with a contact angle of 159° and roll-off angle of 5°.

Representative stress−strain curves in uniaxial tension for untreated, microtextured (60 wt % water), and micro/nanotextured (60 wt % water, 10 wt % silica) PDMS are shown in Figure 5a. The untreated and microtextured samples exhibited a typical elastomeric behavior of low stresses held at low and intermediate strains due to an amorphous structure and easy chain movement, and higher stresses held at high strains once chains were most likely aligned in the tensile direction. Conversely, due to the presence of silica nanoparticles in the pore walls, the micro/nanotextured monolith exhibited a more rigid behavior. Young's moduli (taken over the first 20% of strain) were found to be 0.90 ± 0.05, 0.80 ± 0.04, and 2.00 ± 0.1 MPa for the untreated, microtextured, and micro/nanotextured PDMS, respectively. A decrease in maximum strain was observed for both of the porous PDMS samples. This would be expected due to the pores acting as

DOI: 10.1021/acsami.7b15088
ACS Appl. Mater. Interfaces 2018, 10, 2907−2917

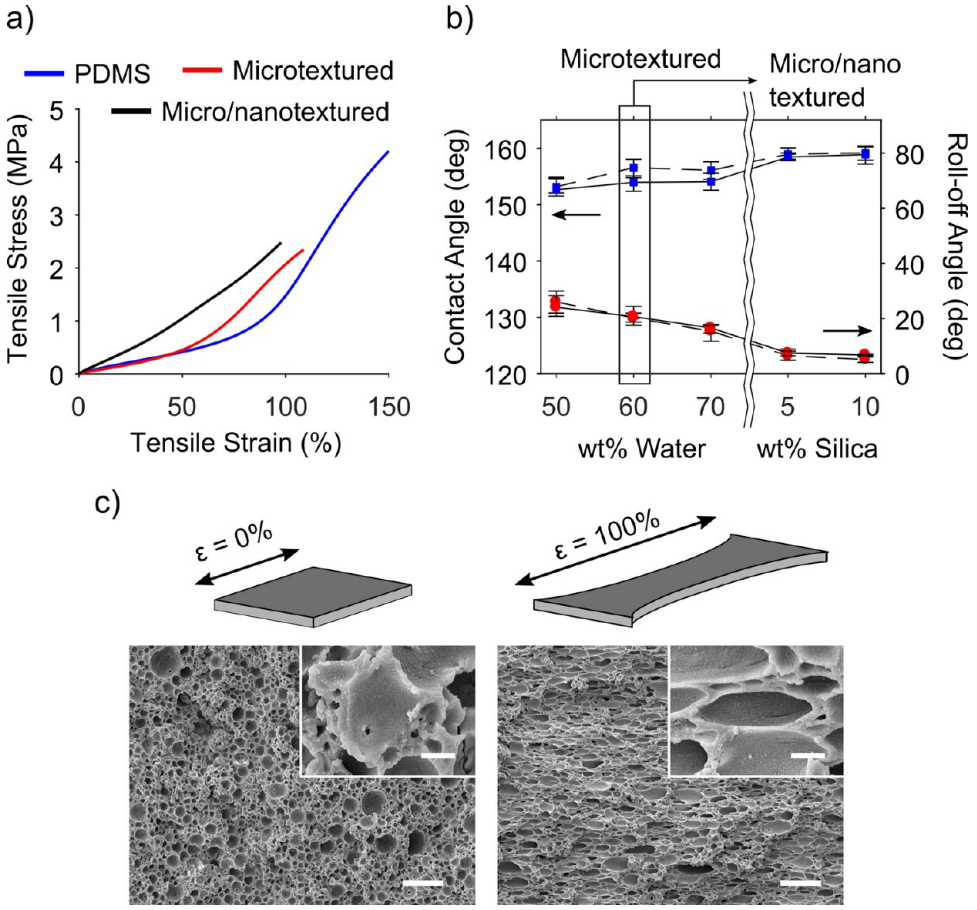

Figure 5. a) Stress−strain curves of untreated, microtextured, and micro/nanotextured PDMS in uniaxial tension. b) Wettability of textured monoliths while nonstretched (dashed lines) and stretched 100% (solid lines). c) SEM images of a micro/nanotextured while nonstretched and stretched 100%. Micropores were observed to stretch along the tensile axis and preserve surface microtexture. Main scale bar = 50 μm. Inset scale bar = 5 μm.

cracks and stress concentrators. Maximum strain was found to be 153 ± 11, 109 ± 5, and 95 ± 10% for the untreated, microtextured, and micro/nanotextured PDMS, respectively. The wettability of several microtextured and micro/nanotextured monoliths was investigated while being uniaxially stretched 100% in a mechanical vise (Figure 5b). Neither contact angle nor roll-off angle were observed to be adversely effected during stretching for any of the monoliths, indicating a stretchable superhydrophobicity. SEM images of a micro/nanotextured silicone monolith while being uniaxially stretched 100% can be seen in Figure 5c. Due to the elastomeric nature of the silicone monoliths, the micropores were observed to stretch along the tensile axis, preserving the microtexture and superhydrophobicity (see Figure S5 for SEM images of uniaxially stretched microtextured monoliths). In addition to uniaxial strain, the contact angle of a microtextured monolith was also observed to remain constant while being subjected to a strain of 50% in both lateral directions (Figure S6 and Movie S1).

A scheme of the wear test described in Section 2.2.4 is shown in Figure 6a. As can be seen in Figure 6b, the microtextured monolith showed a remarkable resistance to mechanical wear by P240 sandpaper, with contact angle remaining practically unchanged before and after the sample was abraded 50 m on the rough surface (156° before, 155° after). Roll-off angle was also observed to be nearly unchanged after 50 m of abrasion when compared to before abrasion (20° before, 22° after). Similarly, the micro/nanotextured monolith showed an essentially equal contact angle (159° before, 161° after) and roll-off angle (5° before, 6° after) when subjected to P240 abrasion. Whereas both samples were able to resist P240 abrasion, a larger difference was observed when abrading using P600 sandpaper. While contact angle remained constant throughout abrasion for both samples, droplets were pinned to the microtextured monolith after 25 m of abrasion, indicating a transition to the Wenzel wetting state. Instead, only a slight increase in roll-off angle was observed to 22° for the micro/nanotextured monolith. The difference in wettability observed after abrading with different sandpaper grits can be explained by examining SEM images of each surface (Figure 6c). While pores were still visibly intact after abrasion with P240 sandpaper, a noticeable flattening of surface features was evident after using P600 sandpaper. Particularly in the case of the microtextured monolith, pores were observed to be nearly completely destroyed, causing the drastic increase in roll-off angle. Instead, the porous structure of the micro/nanotextured monolith was less affected by abrasion, possibly due to a combination of its higher stiffness and nanotexture which remained even after a certain level of microtexture was destroyed. Thus, while the microtextured monolith exhibited wear-similarity when abraded with P240 sandpaper, the micro/nanotextured monolith retained its performance when subjected to abrasion with either P240 or P600 sandpaper (i.e., wear-independent similarity[68]). It should be noted that the

DOI: 10.1021/acsami.7b15088
ACS Appl. Mater. Interfaces 2018, 10, 2907−2917

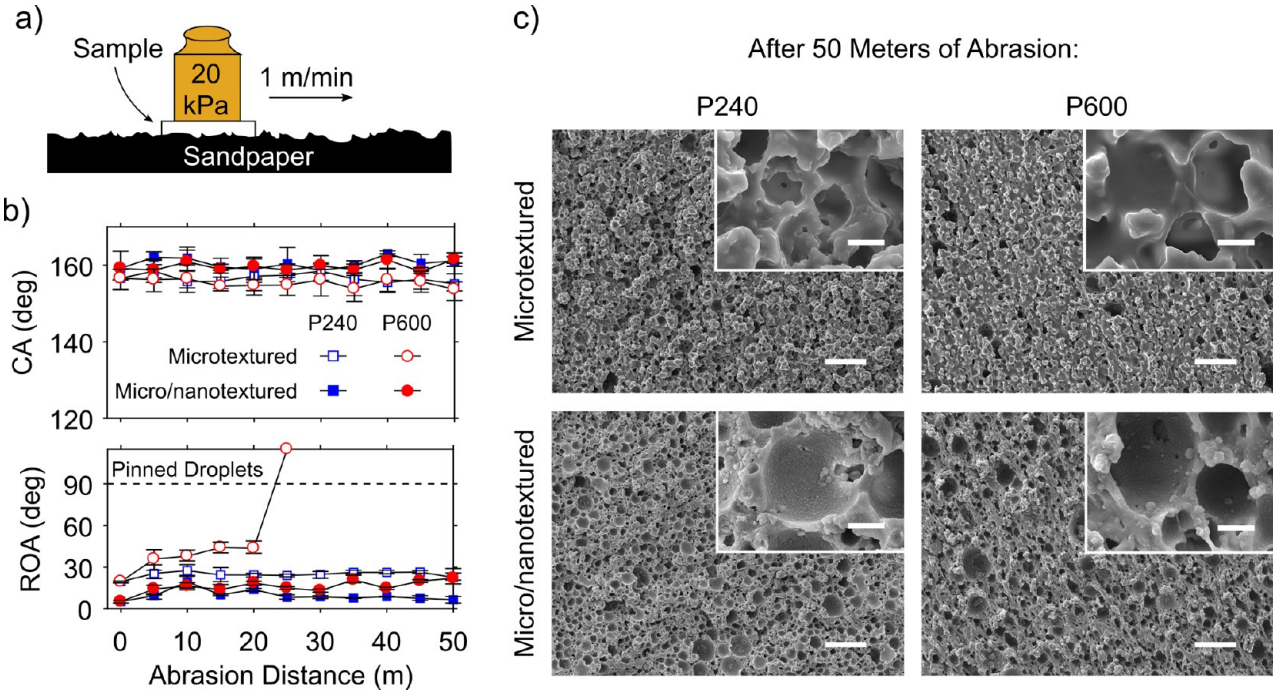

Figure 6. a) Scheme of the wear test used to characterize the abrasion resistance of the micro- and micro/nanotextured monoliths. b) Wettability as a function of abrasion distance using P240 and P600 sandpaper as abradant for each of the surfaces tested. c) SEM images after being abraded with P240 sandpaper revealed the surface texture was nearly the same as a pristine monoliths. After abrasion with P600 sandpaper, the surface morphology appeared more significantly altered, leading to an increase in wettability. Main scale bar = 50 μm. Inset scale bar = 5 μm.

Table 1. Comparison of the Wear-Resistance Exhibited by the Micro/Nano-Textured PDMS Monolith with Previously Reported Superhydrophobic Materials When Subjected to Abrasion by Dragging against Sandpaper

surface	sandpaper grit	pressure (kPa)	distance (m)	final wetting state
silicone resin/silica sol[30]	240	0.54	5	CA = 155°, SA = 3°
structured Al + fluorination[41]	800	4.9	1	CA = 147°
tape + fluorinated TiO_2[31]	240	2.45	8	CA = 155°
PDMS/diatomaceous earth/TiO_2[32]	240	1.4	12	CA = 155°
electrodeposited Zn + fluorinated TiO_2[42]	400	12	0.2	CA = 157.8°, SA = 8°
electrodeposited Ni + stearic acid[33]	800	1.2	0.7	CA = 150°, SA = 53°
epoxy/MgO/TiO_2/stearic acid[34]	1000	3.1	5	CA = 100°, SA = Pinned
concrete/sand/fluoralkylsilane[35]	360	1.1	8	CA = 152°
electrodeposited Ni + fluorination[43]	800	6	1	CA = 148°, SA = 31°
silicone sealant + flame processing[26]	600	24	1	SA = 10°
UHMWPE/SiO_2/NiO[36]	200	2.25	9.65	CA = 160°, SA = 4°
polyester fabric + TiO_2[37]	240	0.51	6	CA = 147°
polystyrene + fluorinated SiO_2[44]	150	7.84	6.75	CA = 152°, SA = 9°
electrodeposited SiO_2 + alkylated SiO_2[38]	1200	0.6	3.4	CA = 149.7°, SA = Pinned
structured Al + SiO_2 + fluorination[39]	400	1.2	1.2	CA = 156°
PU cushion + fluorination + fluorinated TiO_2[45]	600	24	10	CA = 155°
PU spray + silanized palygorskite[40]	2000	2.3	80	CA = 154°, SA = 19°
emulsion templated PDMS (this work)	**240**	**20**	**50**	**CA = 161°, SA = 7°**

combination of pressure and abrasion distance used here is the most strenuous that has so far been reported for testing the wear resistance of superhydrophobic materials (see Table 1 for a comparison of the conditions and results of this work with previous reports).

The robustness of the micro/nanotextured monoliths when subjected to other adverse mechanical treatment and environmental conditions was investigated as can be seen in Figure 7. As a qualitative test of how a superhydrophobic tape might be utilized in real-world situations, knife-scratch, tape-peel (320 N/m), and finger-wipe tests were conducted (Figure 7a, Movie S2). Even after these harsh surface treatments, droplets were observed to roll-away easily at minimal surface tilting. To further test mechanical robustness a compressure pressure of 17 MPa was applied to a superhydrophobic monolith. As can be seen in Figure 7b the microtexture of the monolith was preserved, as were the antiwetting properties (CA = 156°, ROA = 7°). In addition to harsh mechanical treatment, superhydrophobic materials are likely to encounter corrosive liquids in practical applications. As shown in Figure 7c, the silvery sheen of the air layer above the superhydrophobic surface was still clearly visible even when immersed in a highly basic

DOI: 10.1021/acsami.7b15088
ACS Appl. Mater. Interfaces 2018, 10, 2907−2917

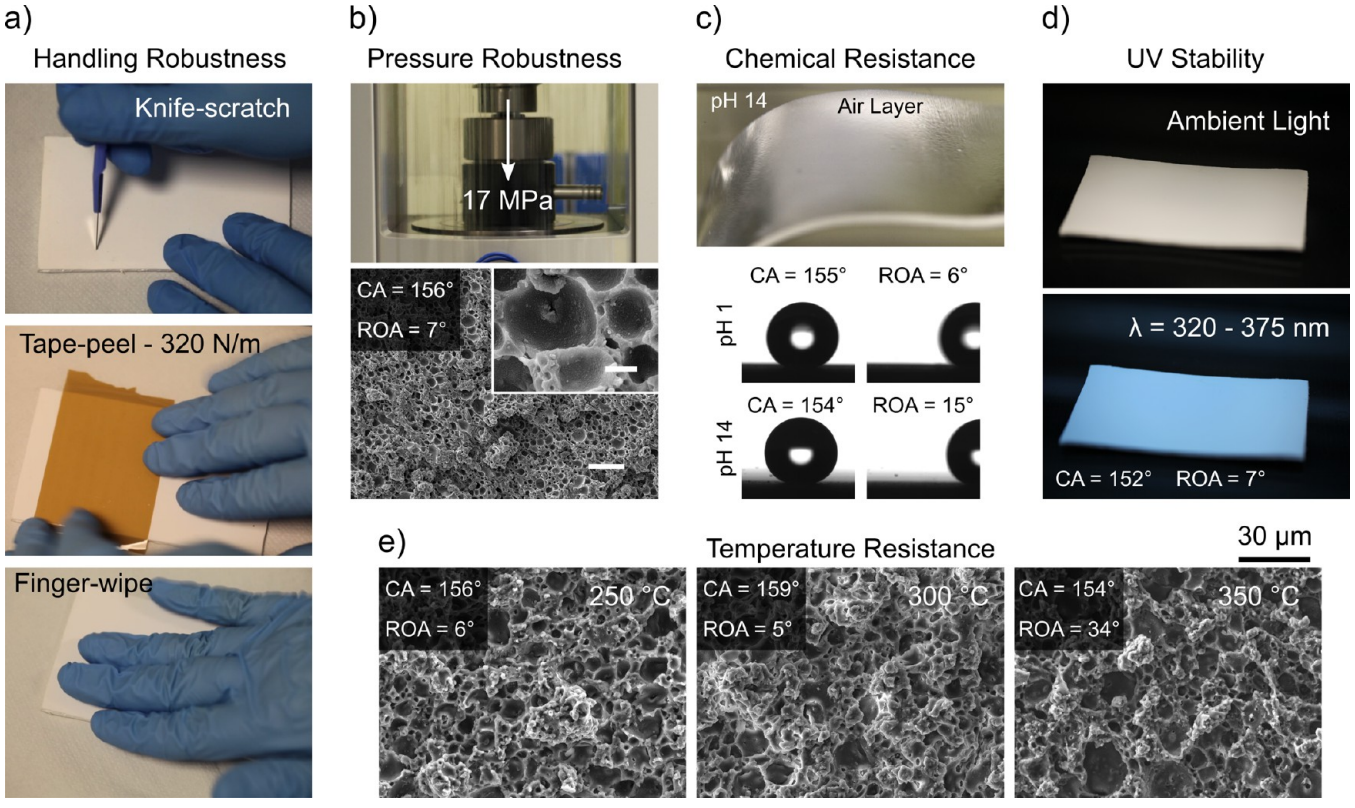

Figure 7. Mechanical and environmental robustness tests performed on the micro/nanotextured monoliths. a) Knife-scratch, tape-peel, and finger-wipe tests to simulate practical handling conditions. b) Compressive pressure test (17 MPa) with surface microtexture and wettability unchanged. c) Photograph of superhydrophobic monolith immersed in highly basic solution with air layer still visible. Wettability after being immersed in highly corrosive solutions. d) Photographs of samples under ambient and UV light. e) SEM images of samples after being heated to extremely high temperatures. Wettability was unchanged when heating up to 300 °C, and droplets were still mobile after heating to 350 °C.

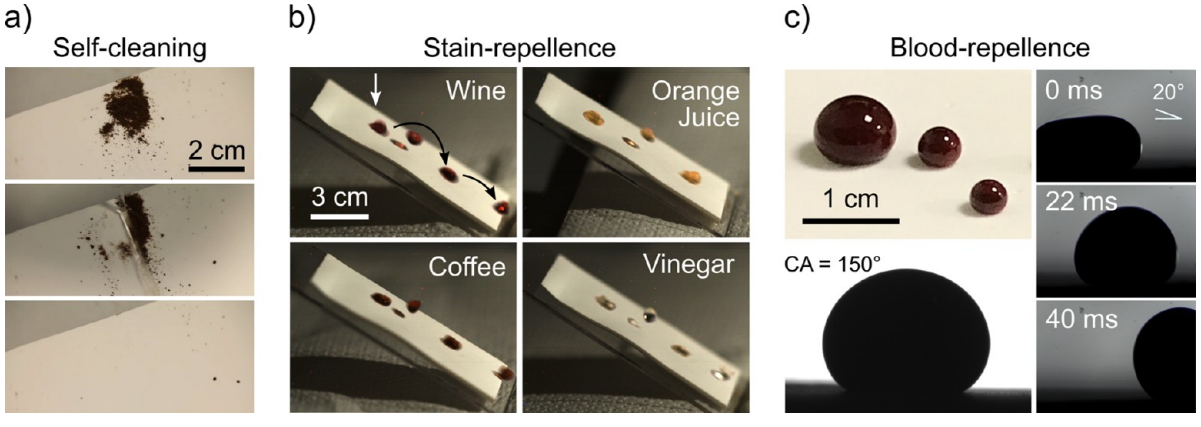

Figure 8. Applications of superhydrophobic micro/nanotextured monoliths: a) Self-cleaning was demonstrated as passing water droplets were easily able to carry away fouling powder spread over the monolith (see Movie S4). b) In addition to water, other commonly encountered liquids were repelled including red wine, coffee, orange juice, and vinegar (see Movie S5). c) Blood droplets were also observed to have mobility, suggesting a possible use as biomedical tubing with reduced flow drag.

solution (pH = 14). The micro/nanotextured monolith showed outstanding resilience after being immersed for 1 h in an acidic solution, with wetting properties unchanged from before immersion. A basic solution was found to cause a slight degradation in roll-off angle to 15°, likely due to remnants of the dispersed NaOH remaining on the surface. UV stability is a particularly important property for potential use in outdoor applications. After being illuminated with UV light for 1 h, the superhydrophobicity of the micro/nanotextured monolith was maintained (Figure 7d). As a final test of environmental stability, wetting properties were examined after samples were heated to extremely high temperatures (Figure 7e). Due to the high temperature stability of PDMS, microtexture remained constant for samples heated up to 300 °C as did wetting properties. A degradation was observed in roll-off angle to 34° for a superhydrophobic sample heated to 350 °C due to thermal degradation of PDMS. Nevertheless, that droplets remained mobile on a sample after being heated to such high temperature indicates that the micro/nanotextured monolith could be used even in applications which require exposure to

DOI: 10.1021/acsami.7b15088
ACS Appl. Mater. Interfaces 2018, 10, 2907−2917

high temperatures. As well as these measures of environmental robustness, a micro/nanotextured sample was able to resist wetting when subjected to high-energy droplet impact (We = 200) as shown in Figure S7 and Movie S3.

In addition to superhydrophobicity, the micro/nanotextured monoliths exhibited several other properties that make them useful for practical applications. As shown in Figure 8a and Movie S4, a fouling agent (cocoa powder) was immediately absorbed by the impacting water droplets, which then easily bounced away from the superhydrophobic surface without leaving any trail behind. Eventually, the surface was cleaned as more water flowed over the surface. Apart from pure water repellence, antiwetting properties with respect to other commonly encountered water-based liquids would also greatly enhance the possible applications of the superhydrophobic monoliths. To test for stain-repellence, ~10 μL red wine, coffee, orange juice, and vinegar droplets were dispensed toward a sample surface from a height of 5 cm, with a composite image of the motion of each of the droplets shown in Figure 8b. As can also be seen in Movie S5, the micro/nanotextured monolith was successfully able to repel all of the test liquids. This stain-repellence is especially impressive for red wine because of its significant ethanol content (12 vol %) which reduces surface tension to approximately 50 mN/m, greatly increasing its ability to wet surfaces. Finally, the biocompatibility of PDMS and flexibility of the superhydrophobic monoliths make them attractive candidates for use as biomedical tubing with reduced friction against passing fluids. Their blood-repellence was thus investigated and can be seen in Figure 8c. Blood droplets were observed to form a nearly spherical shape when placed on a sample surface, with contact angle measured to be 150°. Additionally, when placed on a superhydrophobic surface titled to 20°, droplets were observed to immediately roll away, indicating very low friction between the monolith and the moving droplet.

4. CONCLUSIONS

In this experimental study, robust superhydrophobic materials were fabricated through emulsion templating. This is one of the most environmentally friendly methods yet reported to produce a superhydrophobic material, as it is fluorine-free and VOC-free. Precursor water-in-PDMS emulsions with internal phase fractions as high as 70 wt % produced superhydrophobic microtextured silicone elastomers with well-defined porosities upon cross-linking. Micro/nanotextured monoliths made from precursor emulsions with 60 wt %, incorporating 10 wt % silica nanoparticles with respect to PDMS exhibited the highest superhydrophobicity with a contact angle of 159° and roll-off angle of 5°. Monoliths retained their antiwetting properties even after being subjected to rigorous surface wear and other harsh mechanical treatment and environmental exposure, and demonstrated several useful properties for practical applications including self-cleaning, stain-repellence, and blood-repellence. These results can be useful for the future design and study of scalable and robust superhydrophobic materials.

■ ASSOCIATED CONTENT

Supporting Information

The Supporting Information is available free of charge on the ACS Publications website at DOI: 10.1021/acsami.7b15088.

SEM image of outer layer of porous monolith; optical microscopy and droplet size distribution of water-in-PDMS emulsions; stability of water-in-PDMS emulsions; SEM images of PDMS/iron(III) oxide and PDMS/alumina nanocomposites; SEM images of uniaxially stretched microtextured monoliths; wetting behavior of biaxially stretched microtextured monoliths; and high-speed video frames of resistance to droplet impact at We = 200 (PDF)

Movie S1: Biaxially stretched microtextured monoliths repelling water (AVI)

Movie S2: Knife-scratch, tape-peel, and finger-wipe resistance (AVI)

Movie S3: High-speed video of droplet impact resistance at We = 200 (AVI)

Movie S4: Self-cleaning behavior of superhydrophobic monolith (AVI)

Movie S5: Stain-repellence of superhydrophobic monolith when impacted with red wine, coffee, orange juice, and vinegar droplets (AVI)

■ AUTHOR INFORMATION

Corresponding Authors

*E-mail: alexander.davis@iit.it (A.D.).
*E-mail: ilker.bayer@iit.it (I.S.B.).
*E-mail: athanassia.athanassiou@iit.it (A.A.).

ORCID

Alexander Davis: 0000-0002-5667-2231
Gianvito Caputo: 0000-0002-8973-3109

Notes

The authors declare no competing financial interest.

■ ACKNOWLEDGMENTS

Confocal images for this study were acquired at NIC@IIT (Nikon Imaging Center) at Istituto Italiano di Tecnologia, Genova, Italy. The authors acknowledge Dr. Maria E. Genovese for her assistance acquiring the confocal images.

■ REFERENCES

(1) Zhuang, A.; Liao, R.; Lu, Y.; Dixon, S. C.; Jiamprasertboon, A.; Chen, F.; Sathasivam, S.; Parkin, I. P.; Carmalt, C. J. Transforming a Simple Commercial Glue into Highly Robust Superhydrophobic Surfaces via Aerosol-Assisted Chemical Vapor Deposition. *ACS Appl. Mater. Interfaces* **2017**, *9*, 42327−42335.

(2) Shirtcliffe, N. J.; McHale, G.; Newton, M. I.; Zhang, Y. Superhydrophobic Copper Tubes with Possible Flow Enhancement and Drag Reduction. *ACS Appl. Mater. Interfaces* **2009**, *1*, 1316−1323.

(3) Dean, B.; Bhushan, B. Shark-skin surfaces for fluid-drag reduction in turbulent flow: a review. *Philos. Trans. R. Soc., A* **2010**, *368*, 4775−4806.

(4) Nokes, J. M.; Liedert, R.; Kim, M. Y.; Siddiqui, A.; Chu, M.; Lee, E. K.; Khine, M. Reduced Blood Coagulation on Roll-to-Roll, Shrink-Induced Superhydrophobic Plastics. *Adv. Healthcare Mater.* **2016**, *5*, 593−601.

(5) Hoshian, S.; Kankuri, E.; Ras, R. H. A.; Franssila, S.; Jokinen, V. Water and Blood Repellent Flexible Tubes. *Sci. Rep.* **2017**, *7*, 16019.

(6) Draper, M. C.; Crick, C. R.; Orlickaite, V.; Turek, V. A.; Parkin, I. P.; Edel, J. B. Superhydrophobic Surfaces as an On-Chip Microfluidic Toolkit for Total Droplet Control. *Anal. Chem.* **2013**, *85*, 5405−5410.

(7) Elsharkawy, M.; Schutzius, T. M.; Megaridis, C. M. Inkjet patterned superhydrophobic paper for open-air surface microfluidic devices. *Lab Chip* **2014**, *14*, 1168−1175.

DOI: 10.1021/acsami.7b15088
ACS Appl. Mater. Interfaces 2018, 10, 2907−2917

(8) Ghosh, A.; Ganguly, R.; Schutzius, T. M.; Megaridis, C. M. Wettability patterning for high-rate, pumpless fluid transport on open, non-planar microfluidic platforms. *Lab Chip* **2014**, *14*, 1538−1550.
(9) Wang, L.; Gong, Q.; Zhan, S.; Jiang, L.; Zheng, Y. Robust Anti-Icing Performance of a Flexible Superhydrophobic Surface. *Adv. Mater.* **2016**, *28*, 7729−7735.
(10) Vasileiou, T.; Schutzius, T. M.; Poulikakos, D. Imparting Icephobicity with Substrate Flexibility. *Langmuir* **2017**, *33*, 6708−6718.
(11) Wang, S.; Liu, K.; Yao, X.; Jiang, L. Bioinspired Surfaces with Superwettability: New Insight on Theory, Design, and Applications. *Chem. Rev.* **2015**, *115*, 8230−8293.
(12) Su, B.; Tian, Y.; Jiang, L. Bioinspired Interfaces with Superwettability: From Materials to Chemistry. *J. Am. Chem. Soc.* **2016**, *138*, 1727−1748.
(13) Nishino, T.; Meguro, M.; Nakamae, K.; Matsushita, M.; Ueda, Y. The Lowest Surface Free Energy Based on CF3 Alignment. *Langmuir* **1999**, *15*, 4321−4323.
(14) Russell, M. H.; Berti, W. R.; Szostek, B.; Buck, R. C. Investigation of the Biodegradation Potential of a Fluoroacrylate Polymer Product in Aerobic Soils. *Environ. Sci. Technol.* **2008**, *42*, 800−807.
(15) Milionis, A.; Giannuzzi, R.; Bayer, I. S.; Papadopoulou, E. L.; Ruffilli, R.; Manca, M.; Athanassiou, A. Self-Cleaning Organic/Inorganic Photo-Sensors. *ACS Appl. Mater. Interfaces* **2013**, *5*, 7139−7145.
(16) Alexander, S.; Eastoe, J.; Lord, A. M.; Guittard, F.; Barron, A. R. Branched Hydrocarbon Low Surface Energy Materials for Superhydrophobic Nanoparticle Derived Surfaces. *ACS Appl. Mater. Interfaces* **2016**, *8*, 660−666.
(17) Al-Shatty, W.; Lord, A. M.; Alexander, S.; Barron, A. R. Tunable Surface Properties of Aluminum Oxide Nanoparticles from Highly Hydrophobic to Highly Hydrophilic. *ACS Omega* **2017**, *2*, 2507−2514.
(18) Wang, W.; Lockwood, K.; Boyd, L. M.; Davidson, M. D.; Movafaghi, S.; Vahabi, H.; Khetani, S. R.; Kota, A. K. Superhydrophobic Coatings with Edible Materials. *ACS Appl. Mater. Interfaces* **2016**, *8*, 18664−18668.
(19) Ye, H.; Zhu, L.; Li, W.; Liu, H.; Chen, H. Simple spray deposition of a water-based superhydrophobic coating with high stability for flexible applications. *J. Mater. Chem. A* **2017**, *5*, 9882−9890.
(20) Milionis, A.; Dang, K.; Prato, M.; Loth, E.; Bayer, I. S. Liquid repellent nanocomposites obtained from one-step water-based spray. *J. Mater. Chem. A* **2015**, *3*, 12880−12889.
(21) Chen, K.; Zhou, S.; Yang, S.; Wu, L. Fabrication of All-Water-Based Self-Repairing Superhydrophobic Coatings Based on UV-Responsive Microcapsules. *Adv. Funct. Mater.* **2015**, *25*, 1035−1041.
(22) Chen, K.; Gu, K.; Qiang, S.; Wang, C. Environmental stimuli-responsive self-repairing waterbased superhydrophobic coatings. *RSC Adv.* **2017**, *7*, 543−550.
(23) Schutzius, T. M.; Bayer, I. S.; Qin, J.; Waldroup, D.; Megaridis, C. M. Water-Based, Nonfluorinated Dispersions for Environmentally Benign, Large-Area, Superhydrophobic Coatings. *ACS Appl. Mater. Interfaces* **2013**, *5*, 13419−13425.
(24) Mates, J. E.; Ibrahim, R.; Vera, A.; Guggenheim, S.; Qin, J.; Calewarts, D.; Waldroup, D. E.; Megaridis, C. M. Environmentally-safe and transparent superhydrophobic coatings. *Green Chem.* **2016**, *18*, 2185−2192.
(25) Zhang, X.; Guo, Y.; Chen, H.; Zhu, W.; Zhang, P. A novel damage-tolerant superhydrophobic and superoleophilic material. *J. Mater. Chem. A* **2014**, *2*, 9002−9006.
(26) Tian, X.; Shaw, S.; Lind, K. R.; Cademartiri, L. Thermal Processing of Silicones for Green, Scalable, and Healable Superhydrophobic Coatings. *Adv. Mater.* **2016**, *28*, 3677−3682.
(27) Long, M.; Peng, S.; Yang, X.; Deng, W.; Wen, N.; Miao, K.; Chen, G.; Miao, X.; Deng, W. One-Step Fabrication of Non-Fluorinated Transparent Super-Repellent Surfaces with Tunable Wettability Functioning in Both Air and Oil. *ACS Appl. Mater. Interfaces* **2017**, *9*, 15857−15867.
(28) Zhang, X.; Zhu, W.; He, G.; Zhang, P.; Zhang, Z.; Parkin, I. P. Flexible and mechanically robust superhydrophobic silicone surfaces with stable Cassie-Baxter state. *J. Mater. Chem. A* **2016**, *4*, 14180−14186.
(29) Milionis, A.; Loth, E.; Bayer, I. S. Recent advances in the mechanical durability of superhydrophobic materials. *Adv. Colloid Interface Sci.* **2016**, *229*, 57−79.
(30) Chen, L.; Sun, X.; Hang, J.; Jin, L.; Shang, D.; Shi, L. Large-Scale Fabrication of Robust Superhydrophobic Coatings with High Rigidity and Good Flexibility. *Adv. Mater. Interfaces* **2016**, *3*, 1500718.
(31) Lu, Y.; Sathasivam, S.; Song, J.; Crick, C. R.; Carmalt, C. J.; Parkin, I. P. Robust self-cleaning surfaces that function when exposed to either air or oil. *Science* **2015**, *347*, 1132−1135.
(32) Nine, M. J.; Cole, M. A.; Johnson, L.; Tran, D. N. H.; Losic, D. Robust Superhydrophobic Graphene-Based Composite Coatings with Self-Cleaning and Corrosion Barrier Properties. *ACS Appl. Mater. Interfaces* **2015**, *7*, 28482−28493.
(33) She, Z.; Li, Q.; Wang, Z.; Li, L.; Chen, F.; Zhou, J. Researching the fabrication of anticorrosion superhydrophobic surface on magnesium alloy and its mechanical stability and durability. *Chem. Eng. J.* **2013**, *228*, 415−424.
(34) Si, Y.; Yang, F.; Guo, Z. Bio-inspired one-pot route to prepare robust and repairable micro-nanoscale superhydrophobic coatings. *J. Colloid Interface Sci.* **2017**, *498*, 182−193.
(35) Song, J.; Zhao, D.; Han, Z.; Xu, W.; Lu, Y.; Liu, X.; Liu, B.; Carmalt, C. J.; Deng, X.; Parkin, I. P. Super-robust superhydrophobic concrete. *J. Mater. Chem. A* **2017**, *5*, 14542−14550.
(36) Wang, N.; Lu, Y.; Xiong, D.; Carmalt, C. J.; Parkin, I. P. Designing durable and flexible superhydrophobic coatings and its application in oil purification. *J. Mater. Chem. A* **2016**, *4*, 4107−4116.
(37) Wang, S.; Wu, S.; Zhang, J.; Wang, T. One-step fabrication of recyclable and robust fluorine/polymer-free superhydrophobic fabrics. *RSC Adv.* **2017**, *7*, 24374−24381.
(38) Zhang, X.-F.; Zhao, J.-P.; Hu, J.-M. Abrasion-Resistant, Hot Water-Repellent and Self-Cleaning Superhydrophobic Surfaces Fabricated by Electrophoresis of Nanoparticles in Electrodeposited SolGel Films. *Adv. Mater. Interfaces* **2017**, *4*, 1700177.
(39) Zhang, Q.; Jin, B.; Wang, B.; Fu, Y.; Zhan, X.; Chen, F. Fabrication of a Highly Stable Superhydrophobic Surface with Dual-Scale Structure and Its Antifrosting Properties. *Ind. Eng. Chem. Res.* **2017**, *56*, 2754−2763.
(40) Zhang, J.; Gao, Z.; Li, L.; Li, B.; Sun, H. Waterborne Nonfluorinated Superhydrophobic Coatings with Exceptional Mechanical Durability Based on Natural Nanorods. *Adv. Mater. Interfaces* **2017**, *4*, 1700723.
(41) Li, L.; Huang, T.; Lei, J.; He, J.; Qu, L.; Huang, P.; Zhou, W.; Li, N.; Pan, F. Robust Biomimetic-Structural Superhydrophobic Surface on Aluminum Alloy. *ACS Appl. Mater. Interfaces* **2015**, *7*, 1449−1457.
(42) Qing, Y.; Hu, C.; Yang, C.; An, K.; Tang, F.; Tan, J.; Liu, C. Rough Structure of Electrodeposition as a Template for an Ultrarobust Self-Cleaning Surface. *ACS Appl. Mater. Interfaces* **2017**, *9*, 16571−16580.
(43) Su, F.; Yao, K. Facile Fabrication of Superhydrophobic Surface with Excellent Mechanical Abrasion and Corrosion Resistance on Copper Substrate by a Novel Method. *ACS Appl. Mater. Interfaces* **2014**, *6*, 8762−8770.
(44) Wang, P.; Sun, B.; Yao, T.; Chen, M.; Fan, X.; Han, H.; Li, L.; Wang, C. A novel dissolution and resolidification method for preparing robust superhydrophobic polystyrene/silica composite. *Chem. Eng. J.* **2017**, *326*, 1066−1073.
(45) Zhang, W.; Xiang, T.; Liu, F.; Zhang, M.; Gan, W.; Zhai, X.; Di, X.; Wang, Y.; Liu, G.; Wang, C. Facile Design and Fabrication of Superwetting Surfaces with Excellent Wear-Resistance. *ACS Appl. Mater. Interfaces* **2017**, *9*, 15776−15784.
(46) Verho, T.; Bower, C.; Andrew, P.; Franssila, S.; Ikkala, O.; Ras, R. H. A. Mechanically Durable Superhydrophobic Surfaces. *Adv. Mater.* **2011**, *23*, 673−678.
(47) Xue, C.-H.; Ma, J.-Z. Long-lived superhydrophobic surfaces. *J. Mater. Chem. A* **2013**, *1*, 4146−4161.

DOI: 10.1021/acsami.7b15088
ACS Appl. Mater. Interfaces 2018, 10, 2907−2917

(48) Moglia, R. S.; Holm, J. L.; Sears, N. A.; Wilson, C. J.; Harrison, D. M.; Cosgriff-Hernandez, E. Injectable PolyHIPEs as High-Porosity Bone Grafts. *Biomacromolecules* **2011**, *12*, 3621−3628.
(49) Barbetta, A.; Carnachan, R. J.; Smith, K. H.; Zhao, C.-t.; Cameron, N. R.; Kataky, R.; Hayman, M.; Przyborski, S. A.; Swan, M. Porous Polymers by Emulsion Templating. *Macromol. Symp.* **2005**, *226*, 203−212.
(50) Zhao, C.; Danish, E.; Cameron, N. R.; Kataky, R. Emulsion-templated porous materials (PolyHIPEs) for selective ion and molecular recognition and transport: applications in electrochemical sensing. *J. Mater. Chem.* **2007**, *17*, 2446−2453.
(51) Li, W.; Zhang, W.; Dong, X.; Yan, L.; Qi, R.; Wang, W.; Xie, Z.; Jing, X. Porous heterogeneous organic photocatalyst prepared by HIPE polymerization for oxidation of sulfides under visible light. *J. Mater. Chem.* **2012**, *22*, 17445−17448.
(52) Grant, N. C.; Cooper, A. I.; Zhang, H. Uploading and Temperature-Controlled Release of Polymeric Colloids via Hydrophilic Emulsion-Templated Porous Polymers. *ACS Appl. Mater. Interfaces* **2010**, *2*, 1400−1406.
(53) Manley, S. S.; Graeber, N.; Grof, Z.; Menner, A.; Hewitt, G. F.; Stepanek, F.; Bismarck, A. New insights into the relationship between internal phase level of emulsion templates and gas-liquid permeability of interconnected macroporous polymers. *Soft Matter* **2009**, *5*, 4780−4787.
(54) Deng, X.; Mammen, L.; Zhao, Y.; Lellig, P.; Müllen, K.; Li, C.; Butt, H.-J.; Vollmer, D. Transparent, Thermally Stable and Mechanically Robust Superhydrophobic Surfaces Made from Porous Silica Capsules. *Adv. Mater.* **2011**, *23*, 2962−2965.
(55) Cho, Y.-S.; Choi, S.-Y.; Kim, Y.-K.; Yi, G.-R. Bulk synthesis of ordered macroporous silica particles for superhydrophobic coatings. *J. Colloid Interface Sci.* **2012**, *386*, 88−98.
(56) Wang, R.-k.; Liu, H.-r.; Wang, F.-w Facile Preparation of Raspberry-Like Superhydrophobic Polystyrene Particles via Seeded Dispersion Polymerization. *Langmuir* **2013**, *29*, 11440−11448.
(57) Seo, J.; Lee, S.-K.; Lee, J.; Seung Lee, J.; Kwon, H.; Cho, S.-W.; Ahn, J.-H.; Lee, T. Path-programmable water droplet manipulations on an adhesion controlled superhydrophobic surface. *Sci. Rep.* **2015**, *5*, 12326.
(58) Martin, S.; Bhushan, B. Transparent, wear-resistant, superhydrophobic and superoleophobic poly(dimethylsiloxane) (PDMS) surfaces. *J. Colloid Interface Sci.* **2017**, *488*, 118−126.
(59) Tropmann, A.; Tanguy, L.; Koltay, P.; Zengerle, R.; Riegger, L. Completely Superhydrophobic PDMS Surfaces for Microfluidics. *Langmuir* **2012**, *28*, 8292−8295.
(60) Lee, W.-K.; Jung, W.-B.; Nagel, S. R.; Odom, T. W. Stretchable Superhydrophobicity from Monolithic, Three-Dimensional Hierarchical Wrinkles. *Nano Lett.* **2016**, *16*, 3774−3779.
(61) Hoshian, S.; Jokinen, V.; Franssila, S. Robust hybrid elastomer/metal-oxide superhydrophobic surfaces. *Soft Matter* **2016**, *12*, 6526−6535.
(62) Gong, D.; Long, J.; Jiang, D.; Fan, P.; Zhang, H.; Li, L.; Zhong, M. Robust and Stable Transparent Superhydrophobic Polydimethylsiloxane Films by Duplicating via a Femtosecond Laser-Ablated Template. *ACS Appl. Mater. Interfaces* **2016**, *8*, 17511−17518.
(63) Sahoo, B. N.; Nanda, S.; Kozinski, J. A.; Mitra, S. K. PDMS/camphor soot composite coating: towards a self-healing and a self-cleaning superhydrophobic surface. *RSC Adv.* **2017**, *7*, 15027−15040.
(64) Wang, P.; Chen, M.; Han, H.; Fan, X.; Liu, Q.; Wang, J. Transparent and abrasion-resistant superhydrophobic coating with robust self-cleaning function in either air or oil. *J. Mater. Chem. A* **2016**, *4*, 7869−7874.
(65) Stalder, A.; Kulik, G.; Sage, D.; Barbieri, L.; Hoffmann, P. A Snake-Based Approach to Accurate Determination of Both Contact Points and Contact Angles. *Colloids Surf., A* **2006**, *286*, 92−103.
(66) Tian, X.; Verho, T.; Ras, R. H. A. *Science* **2016**, *352*, 142−143.
(67) Yuan, Z.; Xiao, J.; Zeng, J.; Wang, C.; Liu, J.; Xing, S.; Jiang, D.; Du, G.; Yang, F.; Peng, C.; Chen, H.; Ye, Q.; Tang, J. Facile method to prepare a novel honeycomb-like superhydrophobic Polydimethylsiloxan surface. *Surf. Coat. Technol.* **2010**, *205*, 1947−1952.
(68) Steele, A.; Davis, A.; Kim, J.; Loth, E.; Bayer, I. S. Wear Independent Similarity. *ACS Appl. Mater. Interfaces* **2015**, *7*, 12695−12701.

DOI: 10.1021/acsami.7b15088
ACS Appl. Mater. Interfaces 2018, 10, 2907−2917